Heliyon 10 (2024) e23842

Contents lists available at ScienceDirect

Heliyon

journal homepage: www.cell.com/heliyon

Accelerating stabilization of weathering steel through rust modification pre-corrosion treatment

Qiang Hu [a], Shanwu Yang [a,*], Xu Zhang [b], Guangjie Da [a], Wenhua Zhang [a]

[a] Collaborative Innovation Center of Steel Technology, University of Science and Technology Beijing, Beijing, 100083, China
[b] Research Institute of Technology, Shougang Group Co., Ltd., Beijing, 100043, China

ARTICLE INFO

Keywords:
Weathering steel
Atmospheric corrosion
Rust stabilizing surface treatment
Rust modification
Pre-corrosion

ABSTRACT

To accelerate the formation of the protective rust layer on weathering steel, a new pre-corrosion method containing a replacement reaction was explored. This process was mixed with Cu in the pre-corrosion rust layer to imitate the enrichment of alloying elements through long-term corrosion. By using various analysis methods, the initial corrosion behavior of weathering steel and carbon steel with/without pre-corrosion treatment was studied under indoor wet-dry cycle conditions. The results showed that the pre-corrosion treatment covers the steel surface with a rust layer containing high-concentration Cu. Subsequently, the corrosion uniformity of the weathering steel was significantly improved, and the protective performance of corrosion products was enhanced due to the high concentration of Cu enrichment. This technology is expected to provide a new way to perfect the service performance of weathering steel at the initial stage of application.

1. Introduction

Weathering steel (WS) containing a small amount of alloy elements is a revolutionary product in the field of atmospheric corrosion protection, which has better corrosion resistance and mechanical strength than carbon steel (CS). WS has been applied step by step in civil structures around the world, and its research has been widely attention [1–7].

Abundant pioneer studies indicated that rust layers enriched by alloy elements favor the development of a more compact layer, thereby inhibiting the degradation process of steel. For example, Asami and Kikuchi [8] reported that the rust layer of WS is enriched with Cu, Cr, and Si, which improves the protective ability of steel against a corrosive atmosphere. Yamashita et al. [9] considered that Cr can accelerate the formation of ultrafine goethite with a strongly aggregated structure, which suppresses metal dissolution and corrosive species penetration through the rust layer. W. Wu et al. [10] pointed out that Ni is mainly accumulated in the inner product membrane in the form of $NiFe_2O_4$, which produces the electronegative effect for the inner product membrane to exclude negative chloride ions. In addition, to further enhance the corrosion resistance, applicability, and cost-effectiveness of WS, a mass of excellent work has been executed to optimize the content and composition of alloy elements in the WS [11–15].

However, a dense, well-adhesive protective product film (called patina) enriched in alloying elements needs several years or more of exposure to form gradually [16,17], especially near the substrate, and then the corrosion rate can significantly slow down. The stabilization process of the rust layer is influenced by exposure time, the severity of atmospheric corrosion, and the degree of wet/dry

* Corresponding author.
E-mail address: yangsw@mater.ustb.edu.cn (S. Yang).

https://doi.org/10.1016/j.heliyon.2023.e23842
Received 10 September 2023; Received in revised form 20 November 2023; Accepted 13 December 2023
Available online 16 December 2023

cycling [18,19]. For example, protective rust layers are difficult to form in harsh environments, such as marine atmospheres or salt lake atmospheres [16,20]. In some low-polluting dry environments or sheltered environments lacking dry-wet cycles, steady-state protection layers are also not well developed. In addition, the stabilization process of WS is mainly judged based on the corrosion kinetics [16,21]. Although the appearance, compactness, adhesion, and phase composition of the corrosion products gradually evolve during this process [1,9,22–26], it seems that the accurate definition of rust layer stabilization has not yet established a unified quantitative standard. It can be determined that similar to the atmospheric corrosion of CS, the corrosion products of WS are usually loose and accompanied by a large number of microscopic defects before the stabilization of rust layers [27–29]. During this period, the surface of WS frequently presents a poor appearance due to uneven rust spots or rust flow contamination. In addition, the appearance, compactness, thickness, and other protective properties of the rust layer at diverse positions of the steel structure are not uniform due to discrepancies in factors such as wind, rainfall, and sunlight [16,22].

To solve these problems, some surface treatment methods are proposed. Cook and Yamashita [30] developed a vinyl butyral resin coating containing dispersed $Cr_2(SO_4)_3$, which was beneficial to forming a protective rust layer. The Japanese company JFE Steel Corporation [31] proposed an anionic resin coated on the surface of the steel, which can inhibit rust flow but allows an appropriate amount of O_2 and H_2O to penetrate the coating. In the subsequent corrosion process, continuous and dense corrosion products can be formed on the steel substrate. However, these methods essentially belong to coating, and the operation is relatively complex and time-consuming. Some studies try to accelerate the formation of rust layers by spraying water [32], but protective rust layers rich in alloying elements are laborious to produce. It is necessary to explore new surface treatment technology to improve the defects of WS at the initial stage of application, and to facilitate the stabilization process of the rust layer of WS.

In this work, a new pre-corrosion (PC) method containing a replacement reaction was proposed to accelerate the stabilization process of the rust layer on WS. The initial corrosion behavior of WS, CS, and pre-corroded steels (PC-WS, PC-CS) was compared and studied by indoor wet-dry cycles corrosion test.

2. Material and methods

2.1. Preparation of specimens

The chemical composition of the specimens used in the experiment is presented in Table 1. The experimental steel was cut into three different sizes to perform various characterizations. The steels tested were cut into three different sizes for the indoor wet-dry cyclic corrosion test (CCT). Three parallel samples of 60 mm × 40 mm × 4 mm were used to measure the weight gain in the corrosion process. Specimens of this size are also used to assess the hydration-dehydration capability of the rusted samples. Samples of 20 mm × 10 mm × 4 mm were used for rust layer analysis. For the electrochemical measurements, samples of 10 mm × 10 mm × 4 mm were used, and the wires for the electrical connections were soldered on the samples. All specimens were embedded in resin, and only one side was reserved for testing, as presented in Fig. 1. The exposed surfaces of each sample were mechanically ground with 1000-grit SiC paper. After being cleaned with ethanol, the samples were stored in a desiccator for future use.

The solution used for the PC treatment contains approximately 0.3 wt% NaCl and 0.3 wt% $CuCl_2$, which was sprayed to form an initial rust layer on the steel surface. After surface spray treatment, Fe undergoes a substitution reaction with Cu^{2+} in the PC solution, and Cu precipitates in the pre-corrosion rust layer, as follows:

$$Fe + Cu^{2+} \rightarrow Fe^{2+} + Cu \quad (1)$$

After multiple spray treatments, a pre-corroded rust layer doped with Cu was formed on the steel. Gently rinse the specimen with deionized water and then dry it immediately. The specimens were stored in a dryer for corrosion testing.

2.2. Wet-dry cyclic corrosion test

Fix the specimen with a bamboo stick and place it at a 45° angle to the horizontal plane [16,33], as presented in Fig. 1. Specimens underwent the wet-dry cyclic corrosion test (CCT) [34,35]: (1) The weight gain was obtained through an analytical balance; (2) spraying the specimen surfaces with 0.5 wt% NaCl solution; (3) Place in a room at 10 °C and 50 % RH (relative humidity) for 12 h; (4) Perform steps 2 and 3 again; (5) Weigh the specimen; (6) Rinse the specimen with deionized water to prevent the accumulation of NaCl, followed by immediate drying; (7) Repeat the above process.

2.3. Rust analysis

The morphology of the rust layer was analyzed by scanning electron microscope (SEM), which used the backscatter mode. The element contents and distribution maps in various areas of corrosion products were measured by an energy dispersive spectrometer

Table 1
Chemical composition of CS and WS specimens was studied in this study (wt.%).

Element	C	Si	Mn	P	S	Cu	Ni	Cr	Mo + Ti + Nb	Fe
CS	0.16	0.28	0.62	0.017	0.025	≤0.03	–	–	–	balance
WS	0.09	0.29	1.58	0.009	0.008	1.02	1.28	0.39	≤0.7	balance

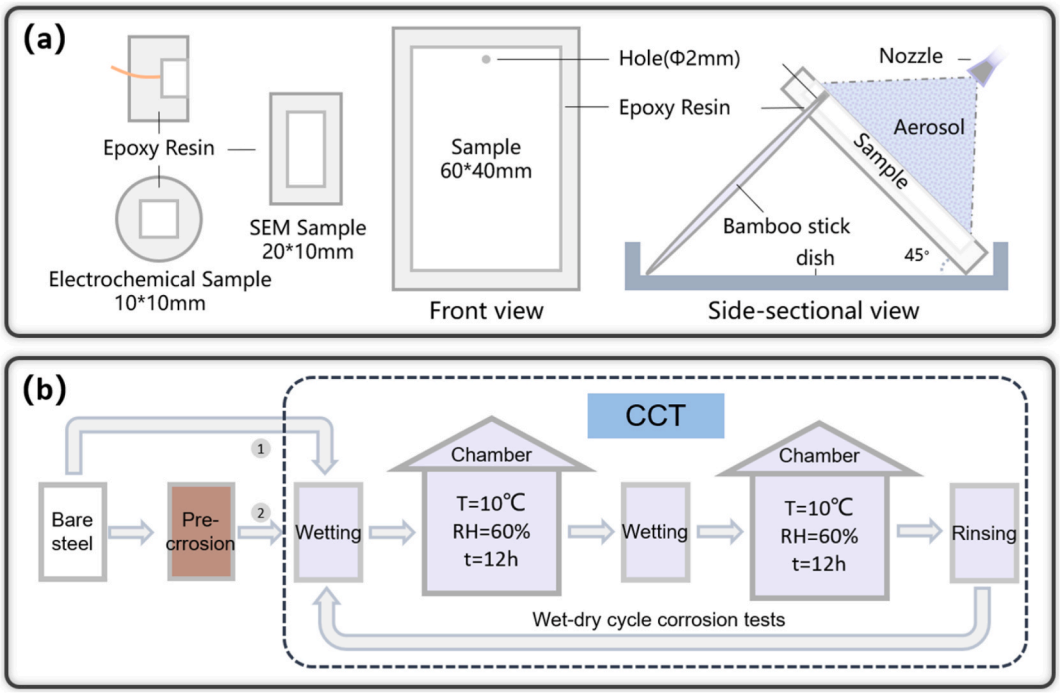

Fig. 1. Schematic diagram of corrosion specimens and wet-dry cycle corrosion tests.

(EDS) and field emission electron probe microanalysis (FE-EPMA). The pre-corroded steel plate was identified by the X-ray diffractometer (XRD) equipped with a Cu target. The scanning rate of 1.5°/min. The SDC350 contact angle tester was utilized to analyze the wettability of the specimen surface. The contact angles at five various positions on the surface of the specimen were tested to obtain an average value. In addition, the existing state of Cu element in the corrosion product was identified by X-ray photoelectron spectroscopy (XPS).

The hydration-dehydration test was conducted on the surface of the specimen [35]. The hydration-dehydration changes of unit area *(GS)* and unit mass *(GM)* were calculated by the following formulas, respectively:

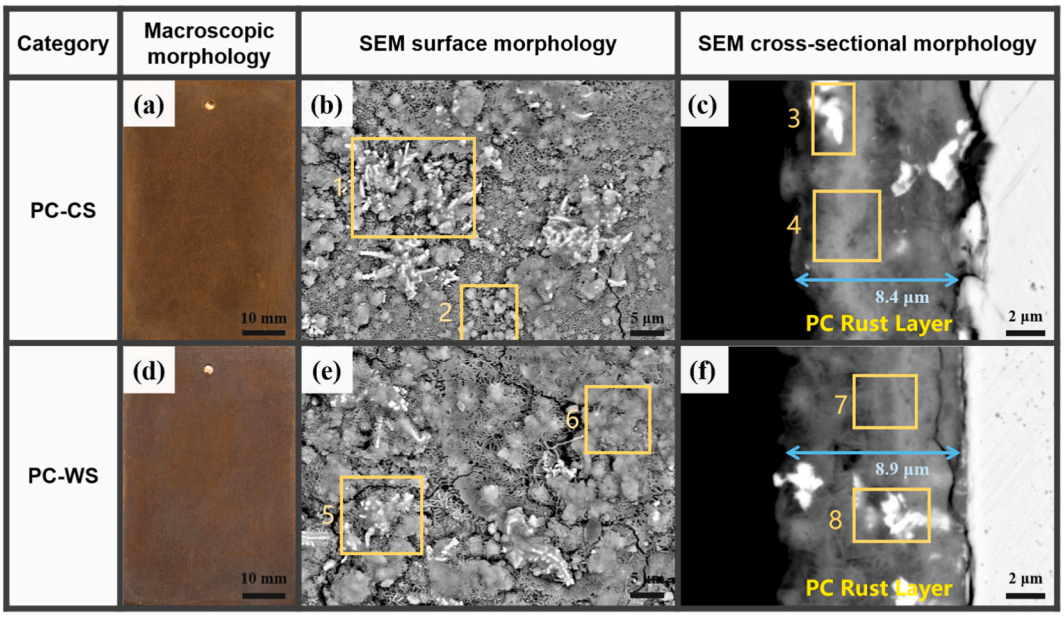

Fig. 2. Morphology of PC-CS and PC-WS samples: (a, d) macroscopic morphology, (b, e) SEM surface morphology, and (c, f) SEM cross-sectional morphology.

$$GS = \frac{(G_t\text{-}G_0)}{S} \tag{2}$$

$$GM = \frac{(G_t\text{-}G_0)}{SW_t} \tag{3}$$

where $(G_t\text{-}G_0)$ represents the weight gain of the rusty specimens after differing water absorption/dehydration time intervals, g; S represents the exposed area of the rusty specimens, cm^2; W_t represents the weight gain per unit area of the corrosion products after the CCT, g.

2.4. Electrochemical measurements

The electrochemical impedance spectroscopy (EIS) measurement was conducted with a VersaSTAT4 electrochemical workstation. The measurement solution is consistent with the corrosion solution mentioned above. Prior to each test, the open circuit potential was stabilized for 30 min. EIS spectrograms were fitted using ZsimpWin commercial software.

3. Results

3.1. Characterization of the pre-corrosion surface layer

Fig. 2a and d shows the macroscopic surface photographs of PC-CS and PC-WS. The specimens are covered with uniform and flat rust layers after PC treatment, which appear brown. From the surface SEM images (Fig. 2b and e) and cross-sectional SEM images (Fig. 2c and f) of the coupons, it can be found that the surface of the steel surface is covered with cobweb-like or cotton ball-like corrosion products and interspersed with granular bright spots. The thickness of the pre-corrosive rust layer on PC-CS and PC-WS is approximately 8.4 μm and 8.9 μm, respectively.

The content (wt.%) of the main elements in diverse local areas of the rust layer is listed in Table 2, which is derived from the EDS analysis (Fig. 3). It can be observed that high concentrations of copper are mixed in the pre-corroded rust layer.

In addition, Fe, O, and Cu surface elements distributed in the pre-corroded rust layer are presented in Fig. 4. It clearly reveals that the bright area in the SEM image of the rust layer is mainly Cu elements. It indicates that the pre-corroded rust layer is randomly doped with copper precipitates at the micron or submicron scale. Interestingly, these precipitations exhibit various shapes, such as dendrite dendrite-like type, agglomerate-like type, and flower-like type, etc., as presented in Fig. 5. The above results indicate that high concentrations of copper are mixed or precipitated in the pre-corroded rust layer.

Fig. 6 represents the XRD spectra of the pre-corroded rust layer on PC-CS and PC-WS. It can be found that Fe, FeOOH, Fe_3O_4, Cu, and CuO are detected in two specimens. The Fe peak in X-ray diffraction is derived from the steel substrate. Combined with SEM and EDS analysis, it can be judged that FeOOH and Fe_3O_4 constituted the matrix of the pre-corrosion rust layer, while Cu and CuO are mixed in the pre-corrosion rust layer.

3.2. Corrosion kinetics

The weight gain per unit surface area of CS, PC-CS, WS, and PC-WS was plotted in Fig. 7a to reflect the corrosion kinetic features. It displays that each weight gain curve rises nearly linearly with corrosion without significant segmentation. Compared to bare steel, pre-corroded specimens exhibit a lower corrosion rate.

The relative corrosion rate (V_x) of various specimens (relative to CS) has been proposed to further demonstrate corrosion resistance. The equation is as follows [13]:

$$V_x = \frac{k_x}{k_{CS}} \times 100\% \tag{4}$$

where k_x and k_{cs} are respectively the slope of the fitting line of the weight gain of specimen and CS. Apparently, the value of a relative corrosion rate V_x ranges from 0 to 100 %. Compared to CS, a lower V_x means the specimen is more resistant to corrosion.

Fig. 7b represents the relative corrosion rates of differing specimens. It conveniently reveals that the value of $V_{PC\text{-}WS}$ is 61.3 % and is the lowest among all specimens. The value of V_{WS} is somewhat higher than that of $V_{PC\text{-}CS}$, while it is notably lower than that of V_{CS}. This means that the corrosion resistance of the rust layer containing alloying elements has been improved, regardless of whether it

Table 2
The specific content (wt.%) of the main elements in diverse local areas of PC-CS and PC-WS rust layer.

Position	1	2	3	4	5	6	7	8
Cu/Fe	0.96	0.24	2.32	0.19	0.41	0.09	0.14	1.32
Cu	39.95	14.88	56.81	11.8	22.46	6.13	8.68	46.2
Fe	43.64	61.35	24.49	60.83	54.74	67.62	63.96	35.03
O	15.07	22.16	14.77	23.14	20.18	23.41	23.65	15.86

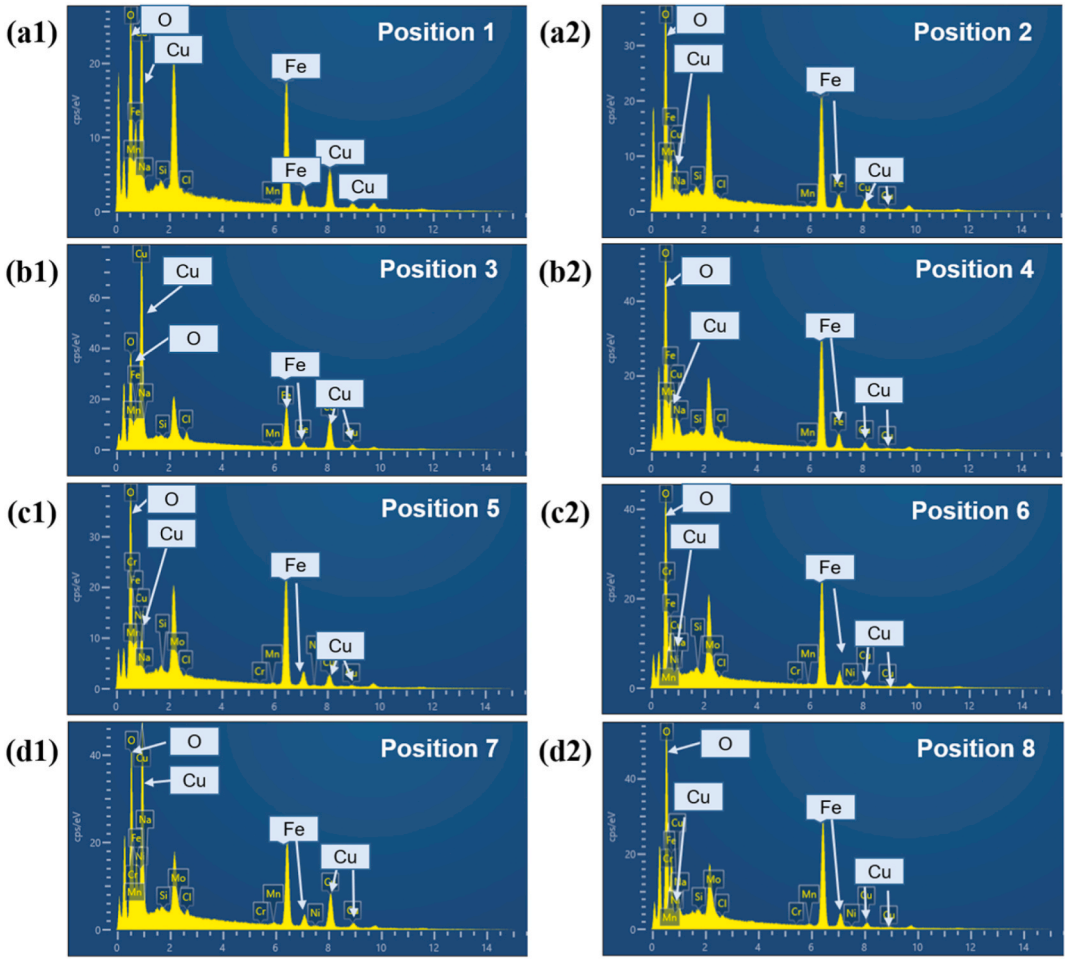

Fig. 3. EDS analysis results in diverse local areas of PC-CS and PC-WS rust layers (yellow frames marked in Fig. 2b, c, e, and f). (For interpretation of the references to color in this figure legend, the reader is referred to the Web version of this article.)

originates from the alloying of steel or the mixing of pre-corrosion rust layers. Besides, the relative corrosion rate of CS or WS treated with PC decreased by 26.0 % and 23.3 %, respectively. Accordingly, the atmospheric corrosion resistance of pre-corroded specimens shows an improvement, and the corrosion products of PC-WS have the best protection for the steel substrate.

Fig. 8 records the appearance evolution of each specimen during the corrosion process. Yellow band rust appeared at the bottom of all specimens because the corrosion liquid flowed down and was stored at the bottom. It should be noted that the appearance evolution on CS and WS is similar. Spotted or striped yellow-orange rust first appears. Subsequently, the rust layer covers the entire specimen little by little, and its color changes to dark brown. However, PC-CS and PC-WS always maintain a uniform dark brown product layer. On the whole, after pre-corrosion treatment, the specimen exhibits a strong inhibitory effect on uneven corrosion.

3.3. *Analysis of corrosion morphology*

To characterize the wettability of the specimen surface, the contact angle of each specimen is tested and the results appear in Fig. 9. Initially, there was a striking discrepancy in contact angles between bare steel and pre-corroded specimens, which were approximately 75° and 25°, respectively. After 60 days, the bare steel contact angle significantly decreased. However, there was no significant change in the contact angle of the pre-corroded specimens. Obviously, in the early stages of the wet-dry cycle, the corrosive liquid on the surface of the bare steel is prone to condense into droplets due to surface tension. On the contrary, the corrosive solution is easier to spread into a homogeneous liquid layer on the surface of the pre-corroded specimens, which is conducive to improving corrosion uniformity. After 60 days, the bare steel contact angle significantly decreased. The contact angle between CS and WS is smaller than that of PC-CS and PC-WS, respectively. This indicates that the rust layer treated with PC has good hydrophobicity, which is beneficial for improving the corrosion resistance of the rust layer.

Fig. 10 shows the surface microstructure of corrosion products after 60 days. All specimens contain rounded protrusions and distributed cracks. Especially, the localized rust layer in CS seems to have warped and will fall off. As can be seen from the specimen

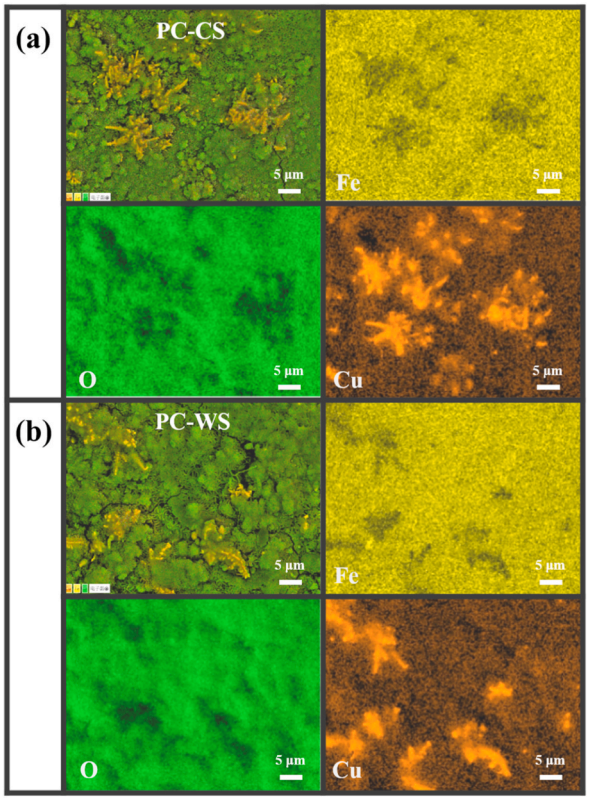

Fig. 4. EDS surface scan results of Fe, O, and Cu.

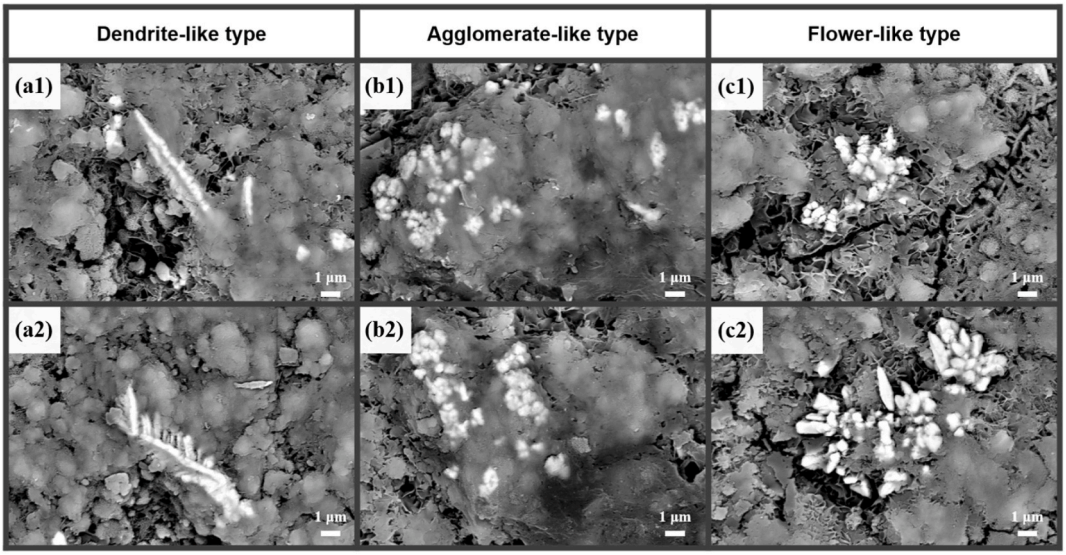

Fig. 5. Typical microscopic morphology of copper precipitation in the pre-corroded rust layer on PC-CS or PC-WS: (a1, a2) Dendrite-like type, (b1, b2) Agglomerate-like type and (c1, c2) Flower-like type.

cross-sectional image in Fig. 11, the rust layer of CS and WS at 30 d is loose and porous. During the subsequent corrosion process, the rust layer becomes dense as the defects are gradually filled with rust particles. As mentioned by Kucera and Mattsson, similar to CS, the rust layer of WS was loose in the early stages of corrosion and became denser with time. In contrast, during the corrosion process, the rust layers of PC-CS and PC-WS exhibit fewer defects and better bond with the substrate. Due to the physical barrier effect of the pre-corrosion layer to a certain extent, it can inhibit the penetration of corrosive solutions into the interior and the transfer of iron ions to

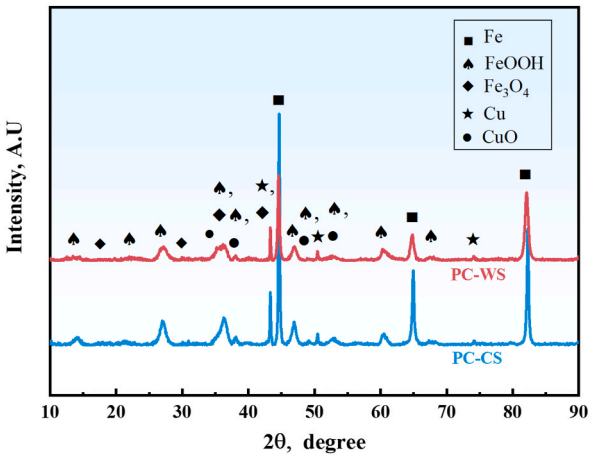

Fig. 6. XRD spectra of the pre-corroded rust layer on PC-CS and PC-WS.

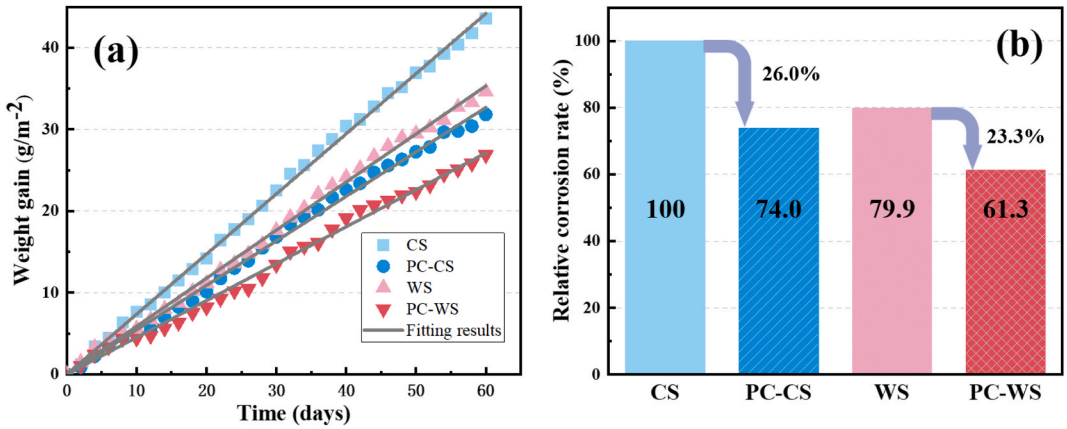

Fig. 7. (a) Corrosion weight gain results and (b) relative corrosion rate of CS, PC-CS, WS, and PC-WS in the corrosion process.

the exterior. Corrosion products are difficult to nucleate and grow freely on the steel surface, resulting in a significant reduction in rust layer defects.

3.4. Results of the hydration-dehydration test

To further clarify the impact of defects in the rust layer, a hydration-dehydration test was conducted on the surface of the specimen, and the results are shown in Fig. 12. From Fig. 12a1 and 12a2, the peak values of the hydration-dehydration curves per unit area/mass of the rust layer in CS and WS are high, while the dehydration rate is slow. This indicates that the bare steel rust layer contains more defects, as the defects absorb water and attenuate the evaporation rate of water [33,35]. As shown in Fig. 12b1, from 30 days to 60 days, the peak values of the hydration-dehydration curves per unit area of CS and WS increased, which may be attributed to an increase in corrosion products. However, the peak value of the hydration-dehydration curve per unit mass of the rust layer decreased for all specimens (Fig. 12b2), indicating that the corrosion products became dense over time. The above results further indicate that pre-corrosion treatment suppressed the generation of defects in the corrosion products, which is consistent with the analysis in Fig. 11.

3.5. Phase composition

The XRD spectra of the corrosion products on various specimens after 60 days are presented in Fig. 13. It can be observed that γ-FeOOH、Fe_3O_4 or γ-Fe_2O_3 are mainly identified on all specimens. The difference in corrosion products between WS and CS is minimal. After pre-corrosion treatment, only magnetite or maghemite peaks slightly increased. Therefore, the pre-corrosion treatment has no significant effect on the rust phases.

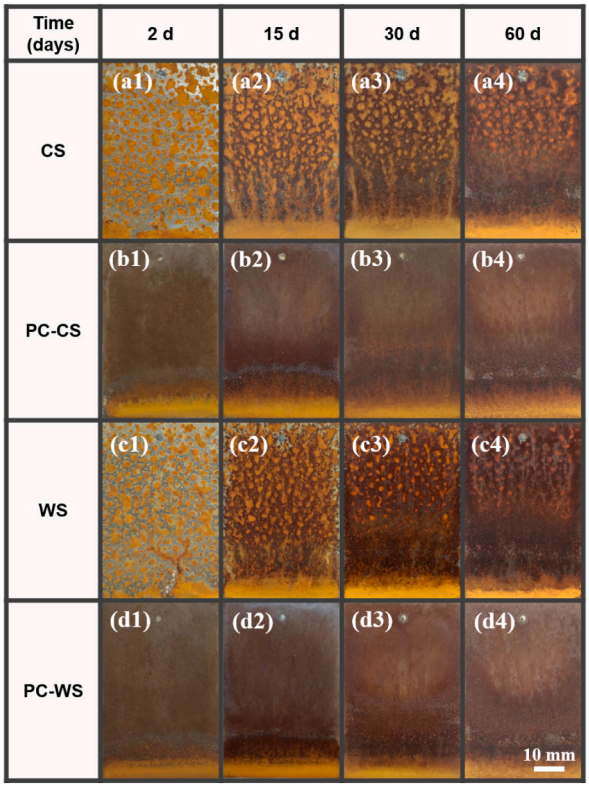

Fig. 8. Appearance evolution process of the rust layer on each specimen: (a1-a4) CS, (b1-b4) PC-CS, (c1-c4) WS, (d1-d4) PC-WS.

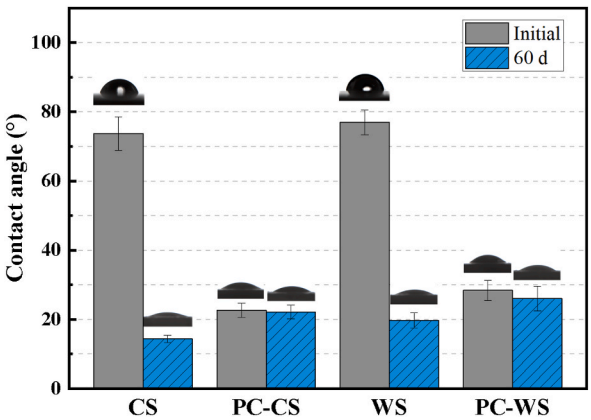

Fig. 9. Contact angle of the surface of each specimen.

3.6. Electrochemical properties

EIS results of the rusted specimens are exhibited in Fig. 14a and b. The spectra consisted of an incomplete semicircle and a long tail, and the high-frequency arc radius increases with corrosion days. Fig. 14d reveals the fitted equivalent circuit. In this figure, R_s represents the resistance of the solution, R_f and C_f represent the resistance and capacitance of the product film, respectively, C_{dl} represents the capacitance of the double layers, R_t represents the charge transfer resistance and Z_w represents the Warburg impedance. The resistance of the rust layer (R_r) is used to evaluate the protective performance of the rust layer [36,37]. Fig. 14c shows the fitted values of R_r for the rusted specimens at 30 and 60 days. The resistance of all rusted specimens increases with the corrosion process. The impedance of the rust layer on CS is the lowest, while the impedance of the rust layer on PC-WS is the highest. In addition, compared to bare steel, pre-corrosion treatment improves the impedance of the corrosion products during the CCT, whether for WS or CS. The copper contained in the corrosion products reduces its conductivity [38]. The results imply the product film on PC-WS presents better

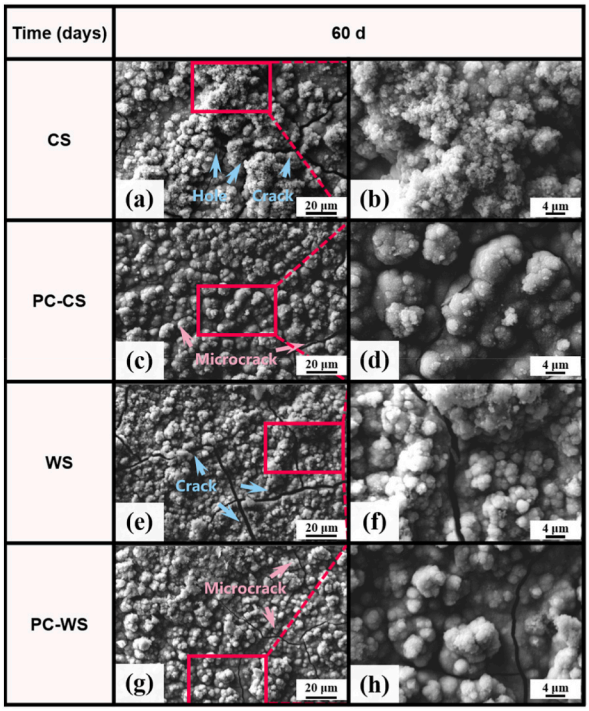

Fig. 10. Surface microstructure of each specimen at 60 days (left), enlarged image (right).

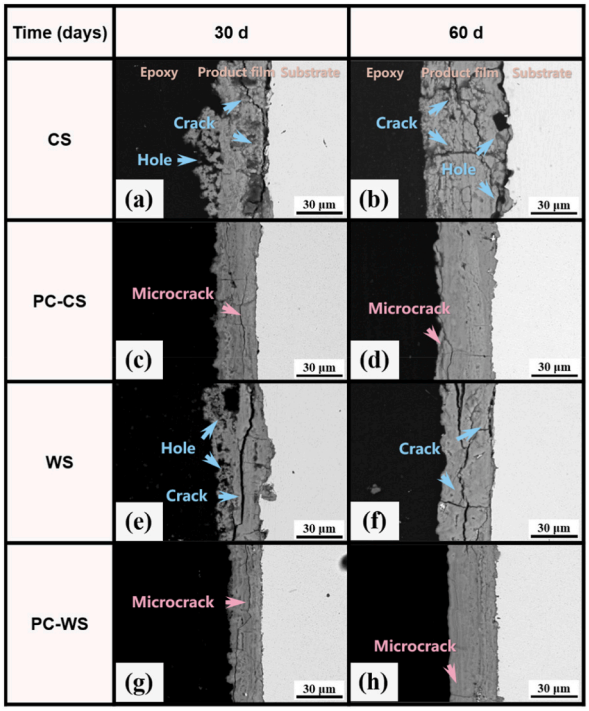

Fig. 11. Cross-sectional morphology of each specimen at 30 and 60 days.

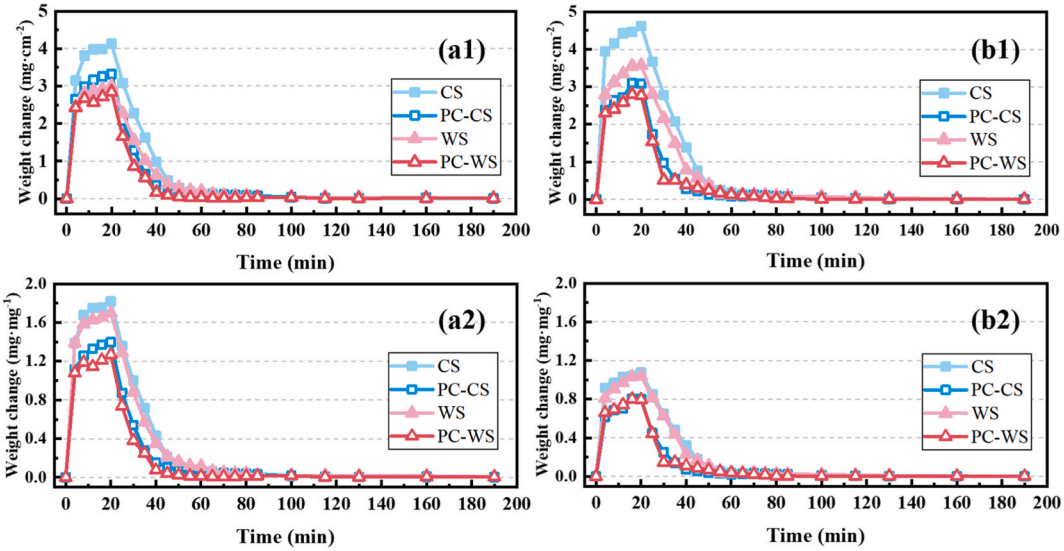

Fig. 12. (a1, b1) Weight change per unit area and (a2, b2) per unit mass of the rusted specimens in hydration-dehydration test on (a1, a2) day 30 and (b1, b2) day 60.

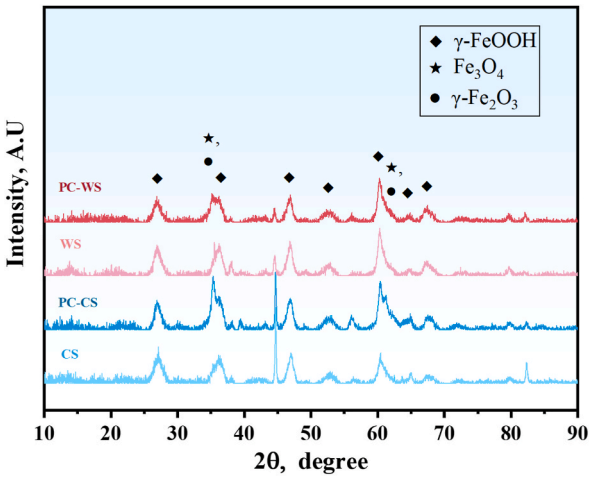

Fig. 13. XRD spectra of corrosion products on various specimens after 60 days.

corrosion resistance.

3.7. *Distribution and existing forms of elements in the rust layer*

Copper is an important corrosion-resistant element, and its content and distribution in the rust layer are closely related to the resistance of the corrosion products [2,39,40]. Given this, 10 various regions of the specimen on day 60 were detected by EDS to reflect the average content and distribution of copper, as shown in Fig. 15a. Since Cu is hardly added to the steel substrate, the rust layer of CS is nearly Cu-free. A high concentration of copper is detected in the rust layer of PC-CS and the peak appeared in the middle layer, because Cu only came from the replacement reaction doping in the pre-corrosion process. For WS, the high content of Cu is only highly concentrated inside near the steel/rust interface. The Cu distribution characteristics of WS and PC-WS are similar, with peaks appearing in the inner layer. However, the Cu content significantly increases in the PC-WS rust layer. The results show that the pre-corrosion treatment improves the Cu enrichment degree of the rust layer of WS in the subsequent corrosion.

To visualize the element enrichment situation more intuitively, EPMA was performed on various cross-section samples, as shown in Fig. 16. The distribution state of Cu in the rust layer roughly reflects the statistical results in Fig. 15. In each sample, Na is uniformly distributed in the rust layer, while the distribution of Cl varies significantly. At higher concentrations of Cl are presented in the inner layer of CS than in the outer layer, which indicates that the corrosion products on CS are difficult to resist the invasion of Cl. This is

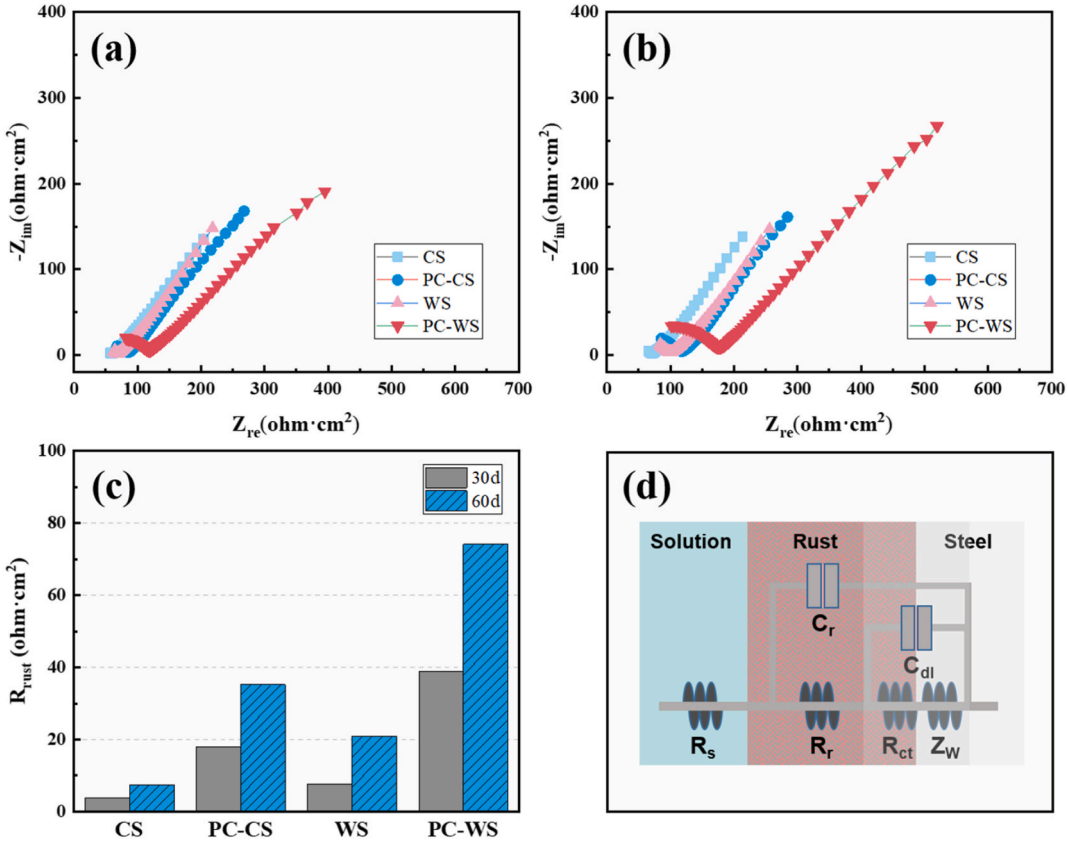

Fig. 14. EIS results of rusted specimens on (a) day 30 and (b) day 60. (c) R_r of the rusted specimens. (d) Equivalent electrical circuit.

consistent with previous studies [33,41,42]. Compared with CS, the concentration of Cl in the WS rust layer is significantly reduced, but the corrosion resistance of the inner layer is still insufficient. Whether it is PC-CS or PC-WS, Cl will be significantly hindered in the outer layer of rust. The difference lies in the fact that pre-corrosion does not change the corrosion characteristics of CS, in which Cl is still enriched in the internal area of corrosion products on PC-CS. The PC-WS exhibits the best corrosion resistance, especially in the inner layer of the corrosion products. In addition, by carefully comparing the distribution of Cu and Cl in each specimen, it can be found that Cl is usually scarce in regions with high concentrations of Cu enrichment. Therefore, the content and distribution of Cu play an important role in the ion-selectivity of the rust layer. The penetration of corrosive electrolytes into the steel matrix can be more effectively prevented by doping the pre-corrosion rust layer with higher levels of Cu.

Fig. 17 shows the XPS spectra of Cu in each specimen. CuO and Cu_2O were identified in all specimens. This indicates that the Cu element exists in the corrosion products in the form of CuO and Cu_2O, whether it is derived from the steel substrate or the pre-corroded rust layer. Based on the corrosion behavior of Cu in an electrolyte solution, the mixed Cu may undergo the following reactions:

$$Cu \rightarrow Cu^{+} + e^{-} \tag{5}$$

$$2Cu^{+} + 2OH^{-} \rightarrow Cu_2O + H_2O \tag{6}$$

$$4Cu^{+} + O_2 + 2H_2O \rightarrow 4Cu^{2+} + 4OH^{-} \tag{7}$$

$$Cu^{2+} + 2OH^{-} \rightarrow CuO + H_2O \tag{8}$$

Firstly, Cu dissolves to form Cu^{+} in an electrolyte solution. Subsequently, one possibility is that it combines with OH^{-} to form Cu_2O. Another possibility is that Cu^{+} is oxidized into Cu^{2+}. According to equation (8), Cu^{2+} will ultimately be transformed into CuO. It can be reasonably inferred that the doped Cu element dissolves and penetrates the rust layer during the subsequent corrosion process, which helps to improve the protective performance of the rust layer.

4. Discussion

The initial atmospheric corrosion of steel is essentially an electrochemical process under the liquid film [43]. The anode of bare steel is active in the initial stage of corrosion. In an electrolyte rich in O_2 and Cl^{-}, the abundant Fe^{2+} will randomly precipitate,

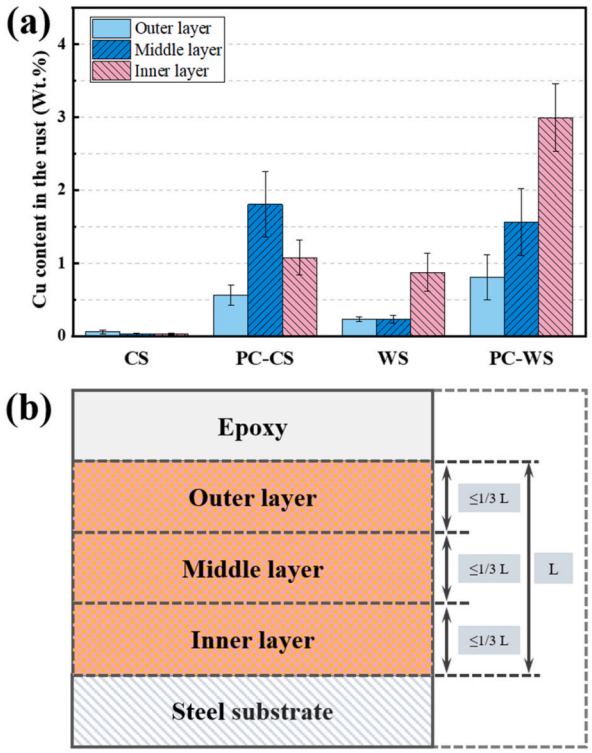

Fig. 15. (a) Content of Cu element in the outer layer, middle layer, and inner layer of the corrosion products after 60 days. (b) Location diagram of EDS selection analysis.

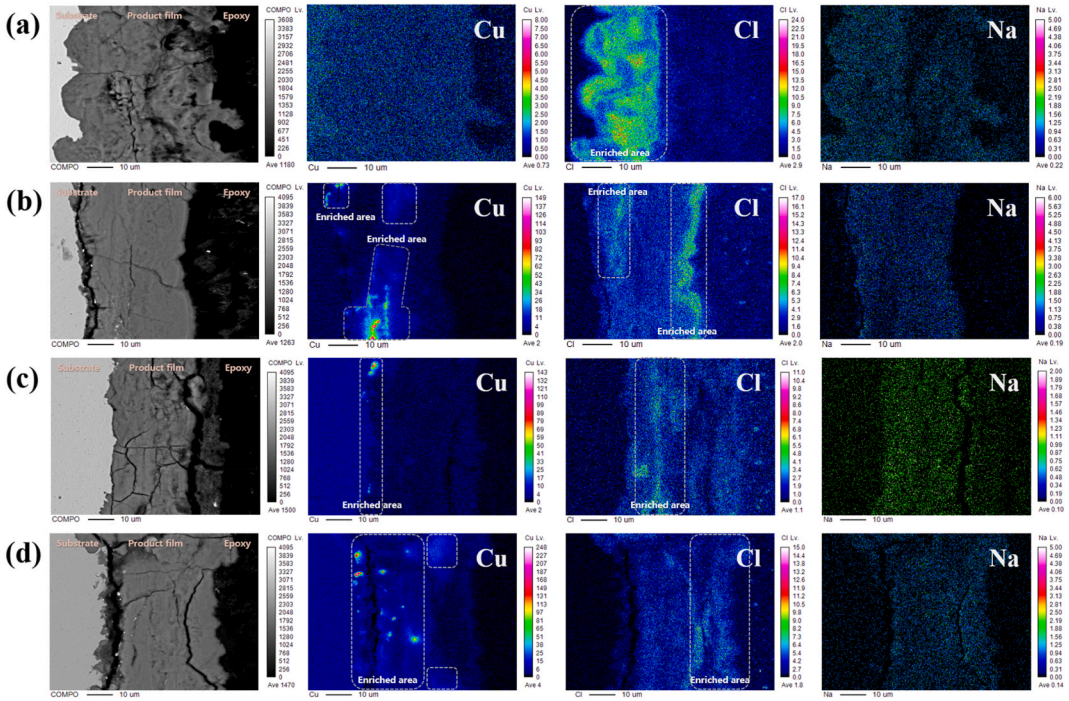

Fig. 16. The element distribution of the corrosion product film generated on the cross-sectional specimens: (a) CS, (b) PC-CS, (c) WS, (d) PC-WS.

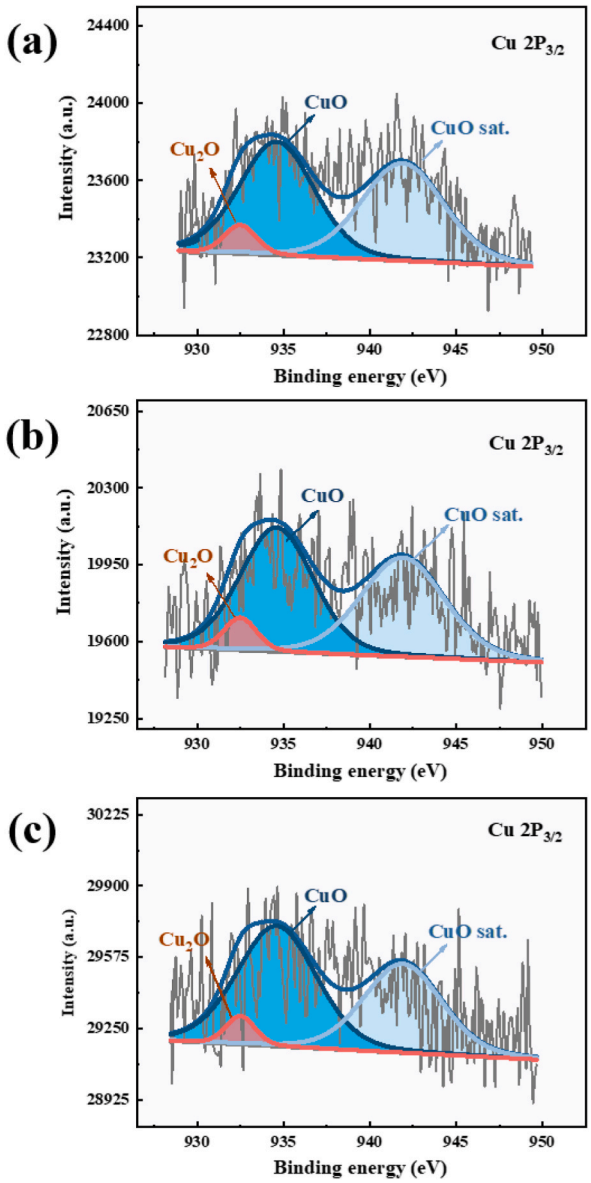

Fig. 17. High-resolution XPS spectra of Cu $2p_{3/2}$ in the corrosion product film generated on the specimens: (a)PC-CS, (b)WS, (c)PC-WS.

aggregate, and eventually grow freely into loose corrosion products on the steel surface (Fig. 11). Since its product film contains a small quantity of alloying elements, which changes the electrical resistance and ionic selectivity to some extent (Figs. 14 and 16), the corrosion rate of WS is lower than that of CS (Fig. 7). However, similar to CS, the initial rust layer of WS still contains abundant defects (Fig. 11). After wetting, the defects in the product film can absorb corrosive liquid and inhibit water evaporation [35,44]. In this case, the wetting time of the steel surface is extended during the wet-dry cycle (Fig. 12). Meanwhile, its high permeability accelerates the adsorption, dissolution, as well as transport of corrosion media such as O_2 or Cl^-, to further aggravate corrosion [43,44]. Therefore, the anti-corrosion effect of WS is limited in the early stages of application, as shown in the mechanism Fig. 18a. In addition, considering factors such as surface wettability and atmospheric deposits, bare steel oftentimes undergoes uneven corrosion in the early stages of application (Figs. 8 and 9).

In the present investigation, a pre-corrosion treatment containing a replacement reaction of Cu is put forward to solve the problem. During the pre-corrosion, rust layer formation and replacement reaction of Cu occur simultaneously. In this way, Cu is doped into rust layers naturally. This exerts two effects on the initial corrosion behavior of WS. On the one hand, pre-corrosion treatment increases the compactness of corrosion products and the content of Cu element (Figs. 11, 12, 15 and 16), which is beneficial for improving impedance and shielding effect on corrosion factors (Figs. 14 and 16) [2,4,40]. On the other hand, pre-corrosion treatment changes the wettability of bare steel, which significantly improves corrosion uniformity (Figs. 8 and 9). Finally, a compact and corrosion-resistant

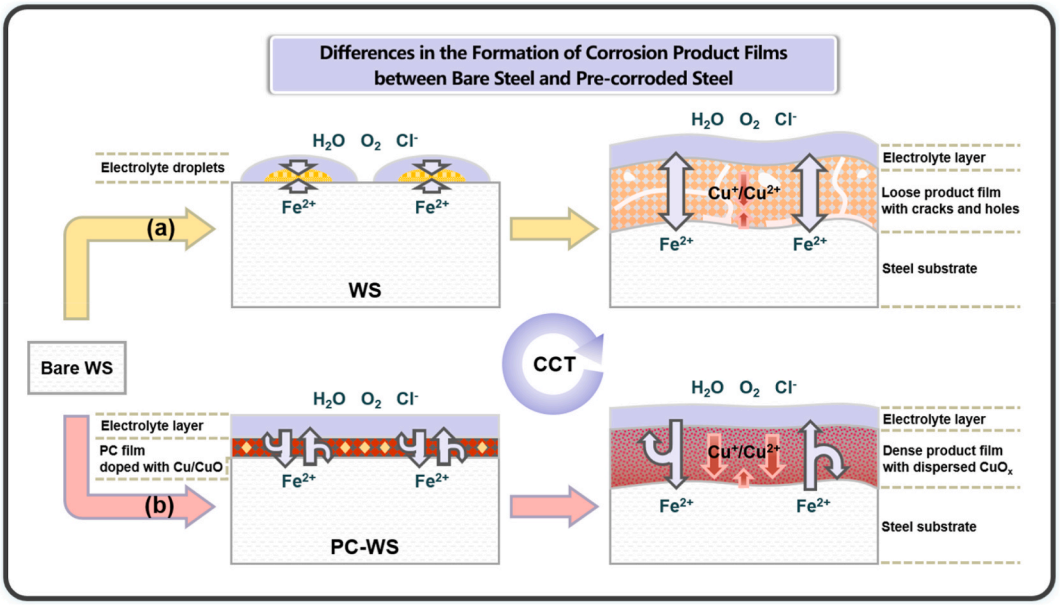

Fig. 18. Mechanism diagram of the evolution process of corrosion product film on (a) WS and (b) PC-WS.

product film is built up on the steel substrate, as shown in Fig. 18b. In addition, only the Cu element was added to explore the pre-corrosion method in this work. If applied in engineering practice, it can be considered to incorporate more alloy elements in the pre-corrosion process to further enhance corrosion resistance.

It should be pointed out that after the pre-corrosion treatment, the improvement of the protection of the rust layer on the CS is a temporary phenomenon. Unlike CS, Cu is not only doped in the pre-corrosive rust layer of WS, but also Cu is promoted to enrich during the subsequent corrosion process. As is seen in Figs. 15 and 16, the Cu peak value occurs in the inner rust layers of PC-WS, which indicates that the Cu in the inner rust layer partially comes from the enrichment effect in subsequent corrosion. Based on the above analysis, it can be considered that the pre-corrosion treatment method of mixed alloy elements is beneficial to the stabilization process of WS.

5. Conclusions

Under the indoor CCT test, the initial atmospheric corrosion behaviors on CS, PC-CS, WS, and PC-WS were compared and analyzed. The main conclusions are as follows:

(1) Both the corrosion rate of CS and WS are reduced through pre-corrosion treatment.
(2) After pre-corrosion treatment with a solution containing Cu^{2+}, the steel surface is covered with a uniform and dense pre-corrosion rust layer mixed with high concentrations of Cu and CuO. The corrosion uniformity of steel structures is significantly improved due to changes in surface wettability during the initial corrosion stage.
(3) The doped Cu is dissolved, penetrated, and formed in the rust layer with CuO or Cu_2O in the subsequent corrosion process. The number of defects and the Cl^- content of the rust layer are significantly suppressed, and the impedance of the rust layer is significantly improved.
(4) The pre-corrosion treatment improves the protection of the rust layer and the further enrichment of alloy elements, which is conducive to the stabilization process of WS.

Additional information

No additional information is available for this paper.

Data availability statement

The research related data was not stored in a publicly available repository. Data will be made available on request.

CRediT authorship contribution statement

Qiang Hu: Data curation, Investigation, Methodology, Writing – original draft. **Shanwu Yang:** Methodology, Writing – review &

editing. **Xu Zhang:** Investigation, Methodology. **Guangjie Da:** Investigation. **Wenhua Zhang:** Investigation.

Declaration of competing interest

The authors declare that they have no known competing financial interests or personal relationships that could have appeared to influence the work reported in this paper.

Acknowledgments

The authors acknowledge the support of the National Key Research and Development Program of China (No. 2017YFB0304700, 2017YFB0304701).

References

[1] M. Morcillo, I. Diaz, H. Cano, B. Chico, D. de la Fuente, Atmospheric corrosion of weathering steels. Overview for engineers. Part I: basic concepts, Constr. Build. Mater. 213 (2019) 723–737.
[2] M. Morcillo, I. Diaz, B. Chico, H. Cano, D. de la Fuente, Weathering steels: from empirical development to scientific design. A review, Corros. Sci. 83 (2014) 6–31.
[3] H. Cano, D. Neff, M. Morcillo, P. Dillmann, I. Diaz, D. de la Fuente, Characterization of corrosion products formed on Ni 2.4 wt%-Cu 0.5 wt%-Cr 0.5 wt% weathering steel exposed in marine atmospheres, Corrosion Sci. 87 (2014) 438–451.
[4] M. Kimura, H. Kihira, N. Ohta, M. Hashimoto, T. Senuma, Control of Fe(O,OH)6 nano-network structures of rust for high atmospheric-corrosion resistance, Corrosion Sci. 47 (2005) 2499–2509.
[5] W.H. Zhang, S.W. Yang, W.T. Geng, Q. Hu, L.J. Zhou, Corrosion behavior of the low alloy weathering steels coupled with stainless steel in simulated open atmosphere, Mater. Chem. Phys. 288 (2022) 11.
[6] P. Lehner, M. Kubzova, V. Krivy, P. Konecny, D. Bujdos, P. Rovnanikova, Correlation between surface concentration of chloride ions and chloride deposition rate in concrete, Constr. Build. Mater. 320 (2022) 11.
[7] A.C. Santa, J.A. Tamayo, C.D. Correa, M.A. Gomez, J.G. Castano, L.M. Baena, Atmospheric corrosion maps as a tool for designing and maintaining building materials: a review, Heliyon 8 (2022) 14.
[8] K. Asami, M. Kikuchi, Characterization of rust layers on weathering steels air-exposed for a long period, Mater. Trans. 43 (2002) 2818–2825.
[9] M. Yamashita, H. Uchida, Recent research and development in solving atmospheric corrosion problems of steel industries in Japan, Hyperfine Interact. 139 (2002) 153–166.
[10] W. Wu, X.Q. Cheng, H.X. Hou, B. Liu, X.G. Li, Insight into the product film formed on Ni-advanced weathering steel in a tropical marine atmosphere, Appl. Surf. Sci. 436 (2018) 80–89.
[11] H. Cano, I. Diaz, D. de la Fuente, B. Chico, M. Morcillo, Effect of Cu, Cr and Ni alloying elements on mechanical properties and atmospheric corrosion resistance of weathering steels in marine atmospheres of different aggressivities, Mater. Corros. 69 (2018) 8–19.
[12] X.Q. Cheng, Z. Jin, M. Liu, X.G. Li, Optimizing the nickel content in weathering steels to enhance their corrosion resistance in acidic atmospheres, Corrosion Sci. 115 (2017) 135–142.
[13] Y.H. Qian, C.H. Ma, D. Niu, J.J. Xu, M.S. Li, Influence of alloyed chromium on the atmospheric corrosion resistance of weathering steels, Corrosion Sci. 74 (2013) 424–429.
[14] C. Liu, R.I. Revilla, Z.Y. Liu, D.W. Zhang, X.G. Li, H. Terryn, Effect of inclusions modified by rare earth elements (Ce, La) on localized marine corrosion in Q460NH weathering steel, Corrosion Sci. 129 (2017) 82–90.
[15] T. Rojhirunsakool, T. Thublaor, M.H.S. Bidabadi, S. Chandra-ambhorn, Z.G. Yang, G.H. Gao, Corrosion behavior of multiphase bainitic rail steels, Metals 12 (2022) 14.
[16] M. Morcillo, B. Chico, I. Diaz, H. Cano, D. de la Fuente, Atmospheric corrosion data of weathering steels, A review, Corros. Sci. 77 (2013) 6–24.
[17] Q.C. Zhang, J.S. Wu, J.J. Wang, W.L. Zheng, J.G. Chen, A.B. Li, Corrosion behavior of weathering steel in marine atmosphere, Mater. Chem. Phys. 77 (2003) 603–608.
[18] X.J. Yang, Y. Yang, M.H. Sun, J.H. Jia, X.Q. Cheng, Z.B. Pei, Q. Li, D. Xu, K. Xiao, X.G. Li, A new understanding of the effect of Cr on the corrosion resistance evolution of weathering steel based on big data technology, J. Mater. Sci. Technol. 104 (2022) 67–80.
[19] S. Syed, Atmospheric corrosion of hot and cold rolled carbon steel under field exposure in Saudi Arabia, Corrosion Sci. 50 (2008) 1779–1784.
[20] J. Wang, Z.Y. Wang, W. Ke, A study of the evolution of rust on weathering steel submitted to the Qinghai salt lake atmospheric corrosion, Mater. Chem. Phys. 139 (2013) 225–232.
[21] R. Vera, B. Valverde, E. Olave, R. Sánchez, A. Díaz-Gómez, L. Muñoz, P. Rojas, Atmospheric corrosion and impact toughness of steels: case study in steels with and without galvanizing, exposed for 3 years in Rapa Nui Island, Heliyon 9 (2023), e17811.
[22] M. Morcillo, I. Diaz, H. Cano, B. Chico, D. de la Fuente, Atmospheric corrosion of weathering steels. Overview for engineers. Part II: testing, inspection, maintenance, Constr. Build. Mater. 222 (2019) 750–765.
[23] T. Ishikawa, M. Kumagai, A. Yasukawa, K. Kandori, Characterization of rust on weathering steel by gas adsorption, Corrosion 57 (2001) 346–352.
[24] J. Monnier, P. Dillmann, L. Legrand, I. Guillot, Corrosion of iron from heritage buildings: proposal for degradation indexes based on rust layer composition and electrochemical reactivity, Corrosion Eng. Sci. Technol. 45 (2010) 375–380.
[25] S. Hara, T. Kamimura, H. Miyuki, M. Yamashita, Taxonomy for protective ability of rust layer using its composition formed on weathering steel bridge, Corrosion Sci. 49 (2007) 1131–1142.
[26] I. Jamil, H. Bano, J.G. Castano, A. Mahmood, Characterization of atmospheric corrosion near the coastal areas of Arabian Sea, Mater. Corros. 69 (2018) 898–907.
[27] Z.F. Wang, P.H. Li, Y. Guan, Q.F. Chen, S.K. Pu, The corrosion resistance of ultra-low carbon bainitic steel, Corrosion Sci. 51 (2009) 954–961.
[28] Y.M. Fan, W. Liu, S.M. Li, T. Chowwanonthapunya, B. Wongpat, Y.G. Zhao, B.J. Dong, T.Y. Zhang, X.G. Li, Evolution of rust layers on carbon steel and weathering steel in high humidity and heat marine atmospheric corrosion, J. Mater. Sci. Technol. 39 (2020) 190–199.
[29] S. Fonna, I. Bin, M. Ibrahim, Gunawarman, S. Huzni, M. Ikhsan, S. Thalib, Investigation of corrosion products formed on the surface of carbon steel exposed in Banda Aceh's atmosphere, Heliyon 7 (2021), e06608.
[30] M.Y.D.C. Cook, High Performance Steels: Properties, Production, Bridges and Corrosion Characteristics, International Workshop on Atmospheric Corrosion and Weathering Steels, Corrosion and Protection group of University of Antioquia, Cartagena de Indias, Colombia, 2004.
[31] H. Nagano, M. Yamashita. Formation of corrosion protective rust on steel exposed to the atmosphere. Available from: http://zkk.co.jp/reppdf/naga1108.pdf.
[32] Q. Yu, Study on Accelerated Stabilization Technology and Long-Term Weatherability Evaluation of the Rust Layer for Weathering Steel, Yanshan University, Qinhuangdao, Hebei, China, 2021.
[33] W. Han, C. Pan, Z.Y. Wang, G.C. Yu, A study on the initial corrosion behavior of carbon steel exposed to outdoor wet-dry cyclic condition, Corrosion Sci. 88 (2014) 89–100.

[34] L. Hao, S.X. Zhang, J.H. Dong, W. Ke, A study of the evolution of rust on Mo-Cu-bearing fire-resistant steel submitted to simulated atmospheric corrosion, Corrosion Sci. 54 (2012) 244–250.
[35] X. Zhang, S.W. Yang, W.H. Zhang, H. Guo, X.L. He, Influence of outer rust layers on corrosion of carbon steel and weathering steel during wet-dry cycles, Corrosion Sci. 82 (2014) 165–172.
[36] J. Guo, S.W. Yang, C.J. Shang, Y. Wang, X.L. He, Influence of carbon content and microstructure on corrosion behaviour of low alloy steels in a Cl- containing environment, Corrosion Sci. 51 (2009) 242–251.
[37] K. Asami, M. Kikuchi, In-depth distribution of rusts on a plain carbon steel and weathering steels exposed to coastal-industrial atmosphere for 17 years, Corrosion Sci. 45 (2003) 2671–2688.
[38] S. Suzuki, K. Shinoda, M. Sato, S. Fujimoto, M. Yamashita, H. Konishi, T. Doi, T. Kamimura, K. Inoue, Y. Waseda, Changes in chemical state and local structure of green rust by addition of copper sulphate ions, Corrosion Sci. 50 (2008) 1761–1765.
[39] Z.F. Wang, J.R. Liu, L.X. Wu, R.D. Han, Y.Q. Sun, Study of the corrosion behavior of weathering steels in atmospheric environments, Corrosion Sci. 67 (2013) 1–10.
[40] J.H. Jia, W. Wu, X.Q. Cheng, J.B. Zhao, Ni-advanced weathering steels in Maldives for two years: corrosion results of tropical marine field test, Constr. Build. Mater. 245 (2020) 9.
[41] J. Alcantara, B. Chico, I. Diaz, D. de la Fuente, M. Morcillo, Airborne chloride deposit and its effect on marine atmospheric corrosion of mild steel, Corrosion Sci. 97 (2015) 74–88.
[42] W. Wu, X.Q. Cheng, J.B. Zhao, X.G. Li, Benefit of the corrosion product film formed on a new weathering steel containing 3% nickel under marine atmosphere in Maldives, Corrosion Sci. 165 (2020) 15.
[43] J. Alcantara, D. de la Fuente, B. Chico, J. Simancas, I. Diaz, M. Morcillo, Marine Atmospheric Corrosion of Carbon Steel: A Review, Materials 10 (2017) 67.
[44] S. Hoerle, F. Mazaudier, P. Dillmann, G. Santarini, Advances in understanding atmospheric corrosion of iron. II. Mechanistic modelling of wet-dry cycles, Corrosion Sci. 46 (2004) 1431–1465.